Hindawi
Journal of Nanomaterials
Volume 2017, Article ID 6702890, 10 pages
https://doi.org/10.1155/2017/6702890

Research Article

Preparation of Fe_3O_4/Reduced Graphene Oxide Nanocomposites with Good Dispersibility for Delivery of Paclitaxel

Xiaojuan Zhang,[1] Wenbin Cai,[1] Lingyun Hao,[1] Suli Feng,[1] Qing Lin,[1] and Wei Jiang[2]

[1]*School of Material Engineering, Jinling Institute of Technology, Nanjing 211169, China*
[2]*National Special Superfine Powder Engineering Research Center, Nanjing University of Science and Technology, Nanjing 210094, China*

Correspondence should be addressed to Lingyun Hao; hly_jit@163.com

Received 13 October 2017; Accepted 5 December 2017; Published 31 December 2017

Academic Editor: Xuping Sun

The Fe_3O_4/reduced graphene oxide (Fe_3O_4/RGO) nanocomposites with good dispersibility were synthesized for targeted delivery of paclitaxel (PTX). Firstly, the superparamagnetic Fe_3O_4/functional GO nanocomposites were prepared via hydrothermal method in which GO sheets were modified by surfactant wrapping. The Fe_3O_4/RGO nanocomposites were successively prepared through the reduction of graphene oxide. The products were investigated by Fourier-transform infrared spectrum, X-ray diffraction, scanning electron microscopy, transmission electron microscopy, thermogravimetric analysis, and vibration sample magnetometry. It was found that spherical Fe_3O_4 nanoparticles were uniformly anchored over the RGO matrix and the nanocomposites were superparamagnetic with saturation magnetization (Ms) of 9.39 emu/g. Then PTX was loaded onto Fe_3O_4/RGO nanocomposites, and the drug loading capacity was 67.9%. Cell viability experiments performed on MCF-7 demonstrated that the Fe_3O_4/RGO-loaded PTX (Fe_3O_4/RGO/PTX) showed cytotoxicity to MCF-7, whereas the Fe_3O_4/RGO displayed no obvious cytotoxicity. The above results indicated that Fe_3O_4/RGO/PTX nanocomposites had potential application in tumor-targeted chemotherapy.

1. Introduction

Paclitaxel (PTX) is used for the first-line chemotherapeutics in breast cancer, lung cancer, and so on [1]. For improving the bioavailability of PTX, some groups made different carriers to load PTX such as hydrogels [2, 3], gel system [4], implantable chitosan film [5], nanogel [6], nanoparticles [7, 8], and nanostructured lipid carrier [9].

The graphene nanocomposites were studied for drug loading and delivery, since the hydrophobic drugs can be loaded on to graphene sheets by π-π stacking. For example, Angelopoulou et al. developed GO/PLA-PEG nanocomposites loading with PTX, which showed satisfactory high loading capacity, controlled release, and cytoxicity against A549 cancer cells [10]. Zhang et al. synthesized PEG modified nano graphene oxide for delivering PTX and indocyanine green (ICG), which had good fluorescence labeling and therapy effect [11].

Moreover, graphene is used as nanoscale building blocks for new nanocomposites because of its unique properties [12–14]. Recent research showed that magnetic nanoparticles (MNPs) could be attached to graphene, which can be applied in magnetic resonance imaging [15], targeted drug delivery [16, 17], biocompatible adsorbent [18], magnetic solid phase extraction [19], microwave electromagnetic [20], Schottky diode applications [21], and biomolecule immobilization [22]. Thus, the bifunctional graphene drug delivery system for magnetic targeting and drug loading was developed in this paper.

In this paper, the magnetic graphene oxide (Fe_3O_4/GO) for delivering PTX was prepared by hydrothermal method, and Fe_3O_4/GO was subsequently reduced to Fe_3O_4/RGO with good dispersibility. The Fe_3O_4/RGO nanocomposites were characterized, and the drug loading and release of PTX were also investigated. Furthermore, the inhibitory effect of Fe_3O_4/RGO-loaded PTX (Fe_3O_4/RGO/PTX) on MCF-7 cells was conducted.

2. Experimental

2.1. Materials. Iron(III) chloride hexahydrate ($FeCl_3 \cdot 6H_2O$), Hexadecyl trimethyl ammonium bromide (CTAB), and

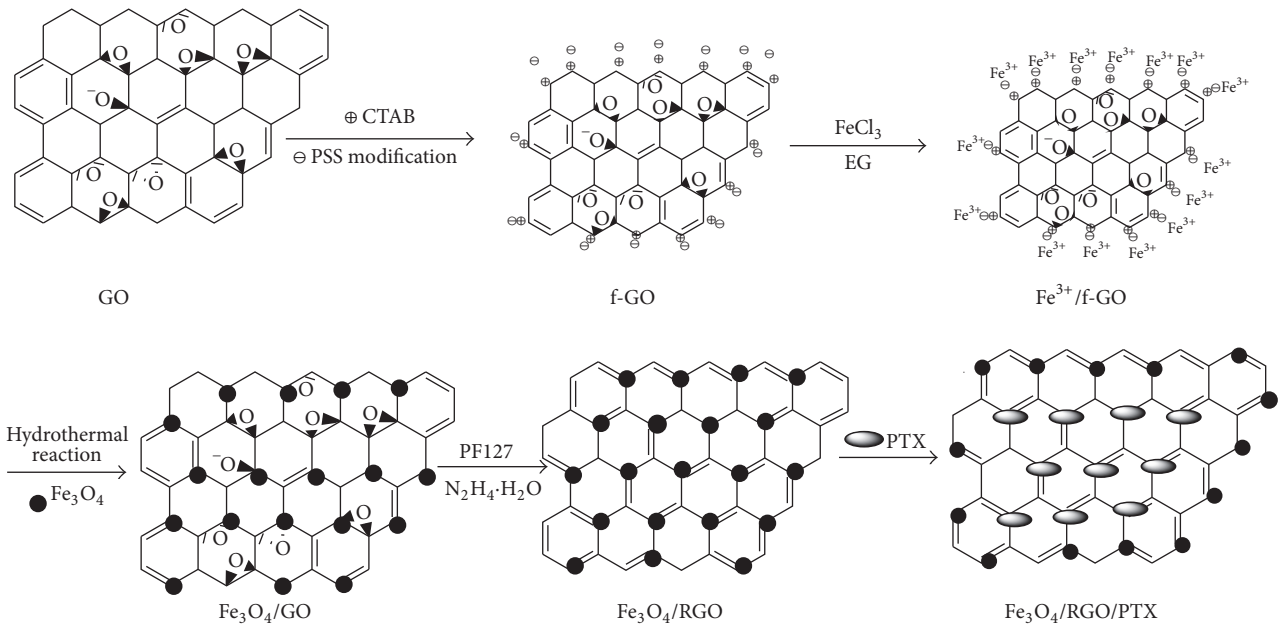

Figure 1: Schematic diagram of the formation processes of PF127/Fe_3O_4/RGO nanocomposites.

Poly(sodium 4-styrenesulfonate) (PSS) were of analytical grade. 3-(4,5-Dimethylthiazol-2-yl)-2,5-diphenyltetrazolium bromide (MTT), PTX, and Triblock copolymers (PEO_{99}-PPO_{67}-PEO_{99}) PF127 were purchased from Sigma. The graphene oxide (GO) was purchased by Xian'feng Nanotechnologies Co. Ltd., China.

2.2. Synthesis and Application of Fe_3O_4/RGO/PTX Nanocomposites. The Fe_3O_4/RGO/PTX nanocomposites synthesis was shown in Figure 1.

2.2.1. Synthesis of Fe_3O_4/RGO/PTX Nanocomposites. To control the particle size of Fe_3O_4 nanoparticles, the GO was modified by the polymer wrapping technique, in which cationic CTAB (1 g) was adsorbed firstly on GO to create a charged template and anionic PSS (0.24 g) was subsequently grafted onto the surfaces of GO (as shown in Figure 1). The mixture of GO modified by CTAB and PSS was obtained, named functional GO (f-GO). The assembly of Fe_3O_4 nanoparticles on f-GO (Fe_3O_4/f-GO) was self-prepared using hydrothermal reaction [23]. For comparison, we synthesized Fe_3O_4/GO without modifying GO.

Secondly, PF127 (400 mg) was dropped to Fe_3O_4/f-GO solution (15 mL, 1.0 mg/mL) and hydrazine monohydrate (400 μL) was then added to reduce the GO [24]. After reaction, Fe_3O_4/RGO nanocomposites were obtained by pressure filtration. Lastly, the PTX was loaded by adding 0.01 g Fe_3O_4/RGO to PBS buffer solution containing PTX (1 mg/mL, 30 mL) at 25°C for 16 h in dark. The suspension was centrifuged and freeze-dried, and Fe_3O_4/RGO/PTX was obtained.

2.2.2. Drug Release of Fe_3O_4/RGO/PTX. The release of Fe_3O_4/RGO/PTX was tested in different buffer (7.4 and 5.0). 10 mg Fe_3O_4/RGO/PTX were suspended in 50 mL buffer at 37°C. The incubated solution (3 mL) was taken out and changed with equal volume buffer. The PTX release was characterized by UV–visible spectrophotometer (UV1101M054) (at 230 nm). The loading efficiency could be calculated by

$$\text{PTX loading efficiency} = \frac{m_d}{m_t} \times 100\%, \quad (1)$$

where m_d is the weight of PTX in the Fe_3O_4/RGO/PTX and m_t is the total weight of Fe_3O_4/RGO/PTX.

2.2.3. Cytotoxicity Assays. Cytotoxicity of free Fe_3O_4/RGO and Fe_3O_4/RGO/PTX was tested on MCF-7 cells. The MTT cell toxicity [25] was measured at 490 nm by enzyme-labeled Instrument (Multiskan FC, Thermo Scientific). Fe_3O_4/RGO and Fe_3O_4/RGO/PTX with different concentrations were added to cells group (six wells) for 24 h, respectively. The fluorescence microscopy of viable cells was characterized by Olympus CKX41.

2.3. Characterization. The structure was characterized by X-ray diffraction (Bruker D8, XRD). Bruker VECTOR 22 spectrometer was used to measure infrared spectrum (IR). The morphology was measured by scanning electron microscopy (Model S-4800, SEM) and transmission electron microscopy (Tecnai 12, TEM). Thermogravimetric analysis was characterized by thermal analyzer (TA2100, America TA). And vibration sample magnetometry (Lake Shore 7410, VSM) was used to detect the magnetic properties.

3. Results and Discussion

3.1. XRD Analysis. As exhibited in Figure 2, the diffraction peak of f-GO appeared at 22.9° which originated from the

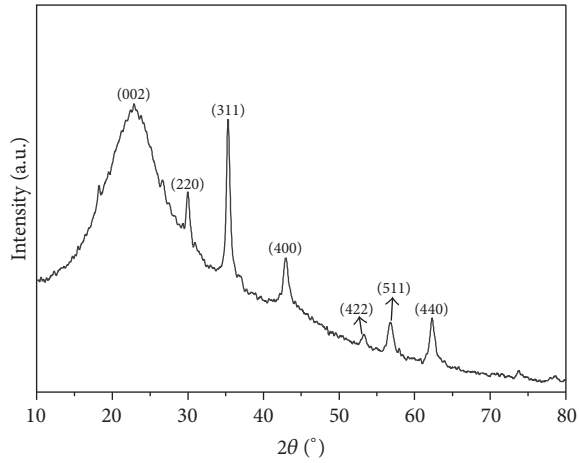

Figure 2: XRD patterns of Fe_3O_4/f-GO.

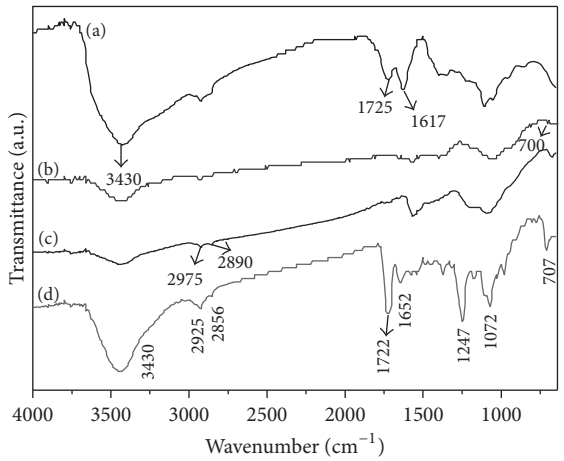

Figure 3: FT-IR spectra of (a) GO, (b) Fe_3O_4/f-GO, (c) Fe_3O_4/RGO, and (d) Fe_3O_4/RGO/PTX.

diffraction on its (002) layer planes [26]. The reflection peaks at 30.1°, 35.4°, 43.1°, 53.5°, 56.9°, and 62.5° can be assigned to (220), (311), (400), (422), (511), and (440) crystal planes of cubic magnetite [27]. It can be concluded that the magnetite-GO heterostructure was formed.

3.2. FT-IR Analysis. The FT-IR spectra for (a) GO, (b) Fe_3O_4/f-GO, (c) Fe_3O_4/RGO, and (d) Fe_3O_4/RGO/PTX were exhibited in Figure 3. In Figure 3(a), the C=O stretching vibration peaks appeared at 1725 cm^{-1}. The peak at 3430 cm^{-1} was assigned to –OH bond, and the C=C bond was exhibited at 1617 cm^{-1}. In Figure 3(b), the Fe–O [28, 29] characteristic band appeared at 700 cm^{-1}. In addition, the bands at 2975 cm^{-1} and 2890 cm^{-1} (Figure 3(c)) could be ascribed to $–CH_3$ and $–CH_2$, which exhibited that Fe_3O_4/RGO was successfully modified by PF127. In Figure 3(d), the peaks at 1072, 1247, 707, 1652, and 1722 cm^{-1} could be ascribed to the C–O ester, –COO, C–H aromatic, C=O amide, and C=O ester [30]. It can be concluded that PTX was loaded on Fe_3O_4/RGO/PTX.

3.3. SEM Analysis. Figure 4(a) showed that the GO had flake structure. After surfactant modification, the f-GO (Figure 4(b)) had good dispersibility. From Figure 4(c), before GO modification, few Fe_3O_4 nanoparticles were supported on the GO nanosheets. After GO modification, Figure 4(d) exhibited that spherical Fe_3O_4 nanoparticles were homogeneously distributed over the GO nanosheets, because the modified GO were covered with a negatively charged polyelectrolyte which can insure homogenous, high-density coverage of positively charged Fe^{3+} by electrostatic attraction. In Figure 4(e), after PF127 modification and reduction, Fe_3O_4 nanoparticles of 100 nm were loaded on the surface of RGO nanosheets. In addition, no free Fe_3O_4 nanoparticles were observed outside of RGO, indicating a strong interaction between Fe_3O_4 nanoparticles and RGO by modification by PF127. In Figure 4(f), it was observed that the Fe_3O_4/RGO/PTX had good morphology and dispersability, which could be applied in subsequent experiments.

3.4. TEM Analysis. Figure 5(a) showed TEM images of f-GO, which exhibited a typical wrinkled morphology and

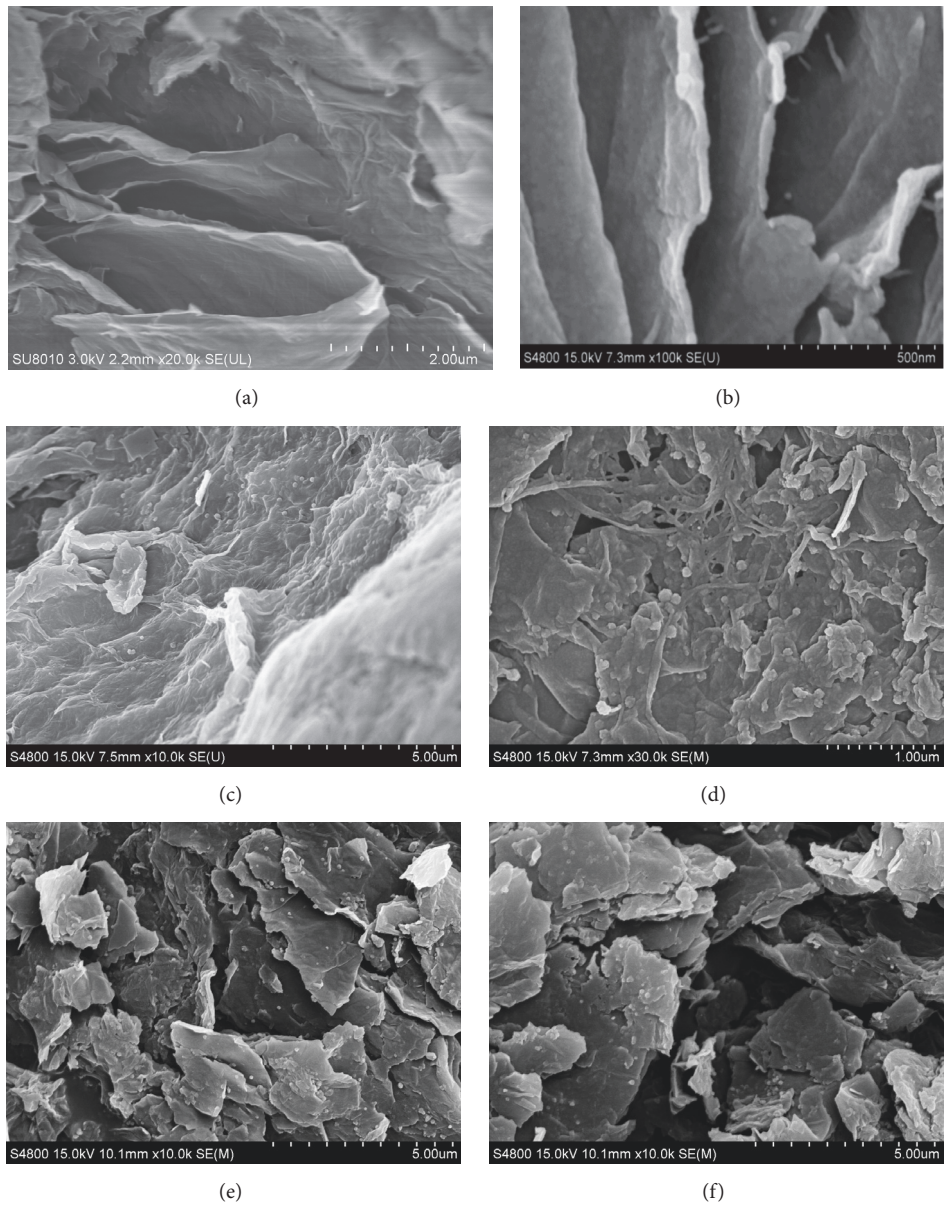

Figure 4: SEM images for (a) GO, (b) f-GO, (c) Fe_3O_4/GO, (d) Fe_3O_4/f-GO, (e) Fe_3O_4/RGO, and (f) Fe_3O_4/RGO/PTX.

good dispersibility. In Figure 5(b), it was found that the GO carbon sheets were decorated by Fe_3O_4 nanoparticles with diameters from 50 nm to 100 nm. From the TEM of Fe_3O_4/f-GO nanocomposites with high resolution (Figure 5(c)), it was exhibited that Fe_3O_4 nanoparticles supported on GO nanosheets had good dispersibility and sphericity. After being modified by PF127 (Figure 5(c)), the Fe_3O_4/RGO nanocomposites had good dispersibility, from which it can be concluded that good dispersibility may be ascribed to the PF127 immobilization. After loading with PTX (Figure 5(d)), Fe_3O_4 nanoparticles were still firmly anchored on the surface of RGO.

3.5. TG Analysis. From Figure 6(a), 40.4% mass loss before 200°C was due to desorption of H_2O and pyrolysis of oxygen-containing group [24]. The pyrolysis of carbon skeleton was exhibited at 50.3% mass loss between 200 and 550°C. Figure 6(b) showed that 17.4% weight loss before 300°C was the removal of labile groups. A further 32.2% weight loss at 400°C (Figure 6(b)) was due to the decomposition of carboxyl group. From Figure 6(c), 3.6% weight loss below 200°C was corresponding to labile oxygen-containing functional groups. A further 32.3% weight loss was observed at around 400°C (Figure 6(c)), which was due to the decomposition of PF127. Finally, 43.1% at around 500°C was ascribed to the carbon skeleton pyrolysis.

3.6. VSM Analysis. In Figure 7(a), the products showed superparamagnetism without any hysteresis [31]. The saturation magnetization (*Ms*) of Fe_3O_4/f-GO was

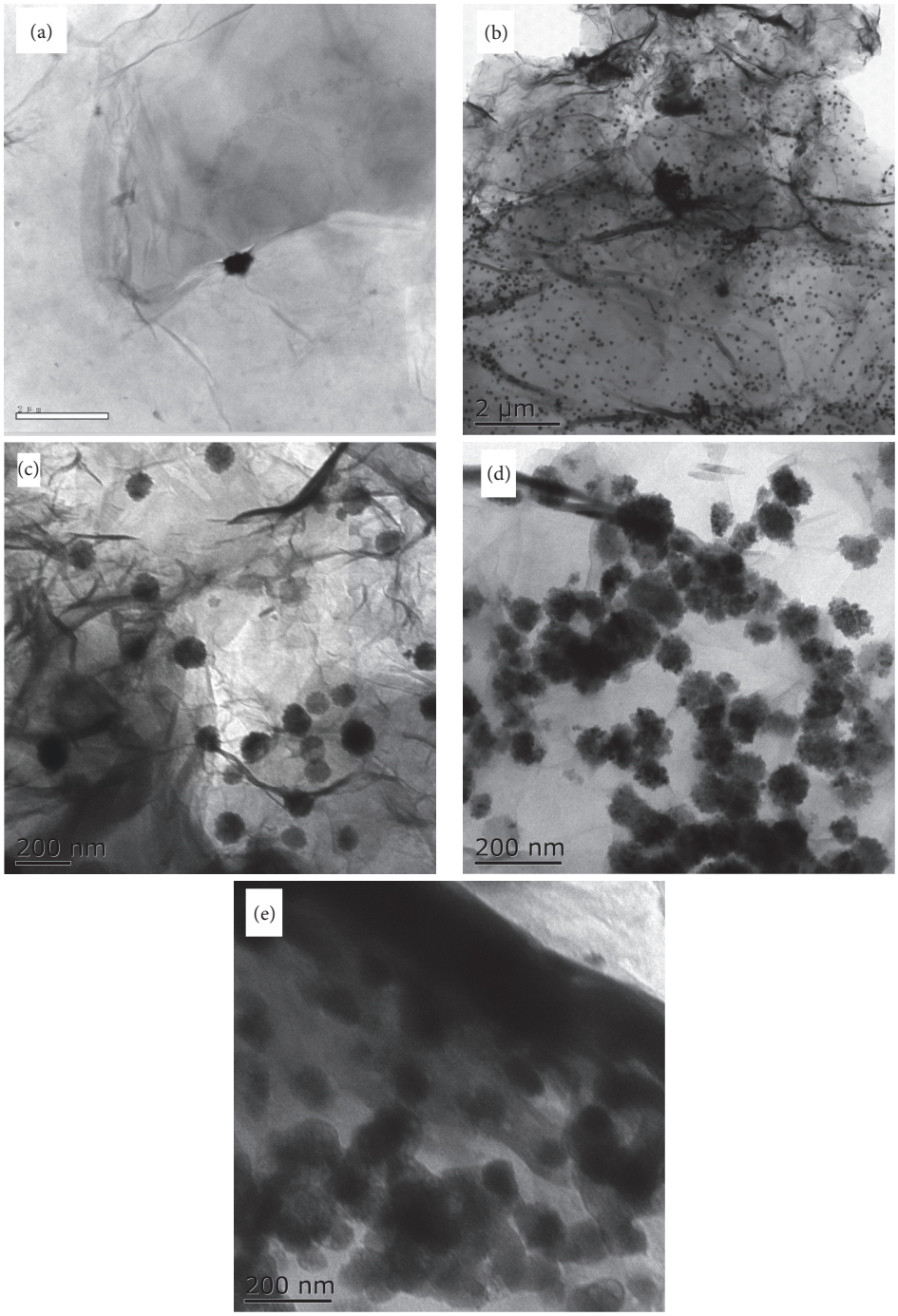

Figure 5: TEM images of (a) f-GO, (b) (c) Fe_3O_4/f-GO, (d) Fe_3O_4/RGO, and (e) Fe_3O_4/RGO/PTX.

9.39 emu/g. Before GO modification, the *Ms* of as-obtained Fe_3O_4/GO nanocomposites decrease to 6.50 emu/g; it was due to the fewer Fe_3O_4 nanoparticles supported on the GO nanosheets. After drug loading, the *Ms* of Fe_3O_4/RGO/PTX was 5.23 emu/g (Figure 7(c)). It could be seen that Fe_3O_4/RGO/PTX maintained good saturation magnetization, which was critical for further application.

3.7. UV Analysis. The release profiles of PTX from Fe_3O_4/RGO/PTX were shown in Figure 8. The standard curve of PTX was (2), and the drug loading efficiency of Fe_3O_4/RGO/PTX was 67.9%.

$$A = 16.032 \cdot C + 0.0766, \quad R^2 = 0.981. \tag{2}$$

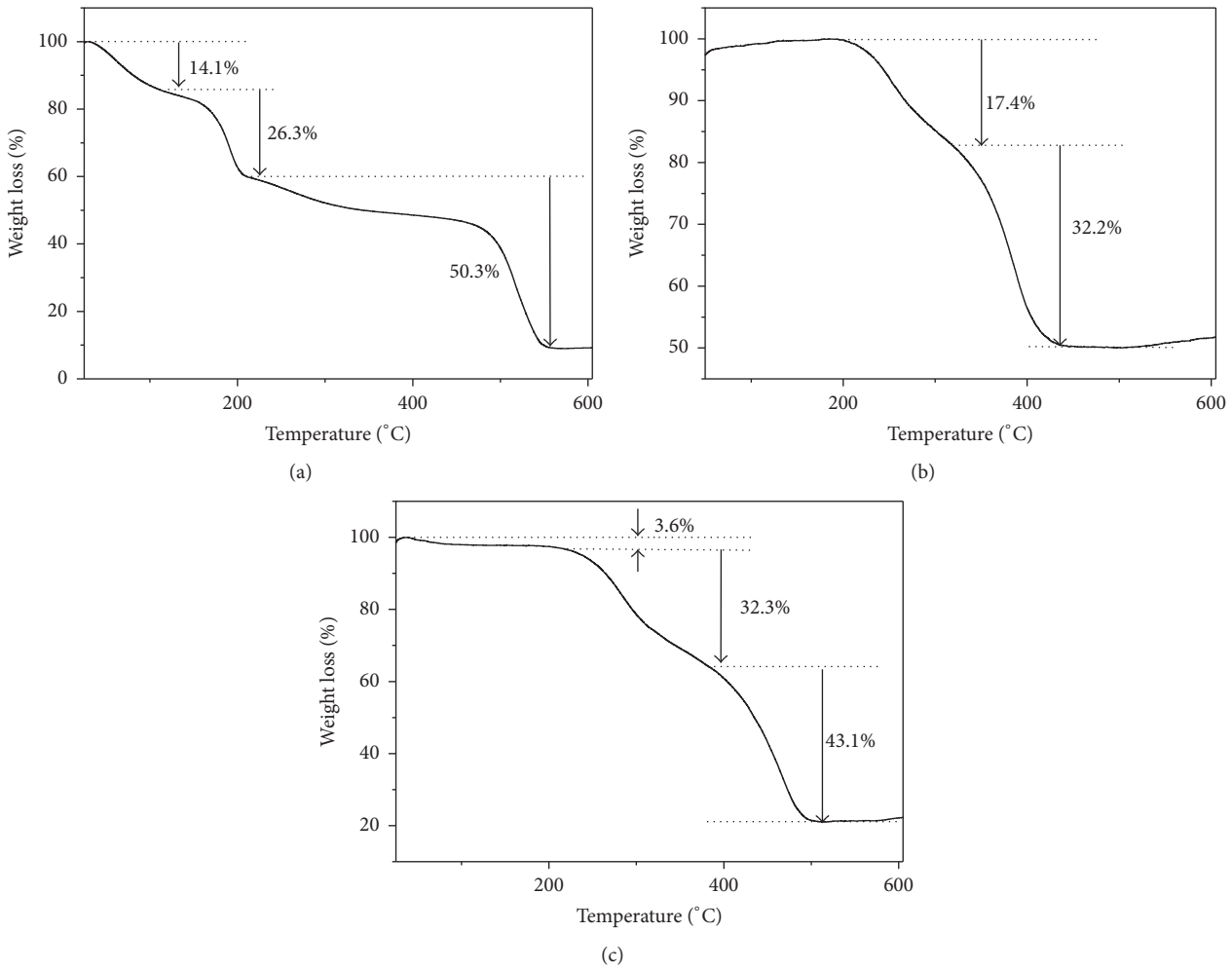

Figure 6: TG curves of (a) GO, (b) Fe_3O_4/f-GO, and (c) PF127/Fe_3O_4/RGO.

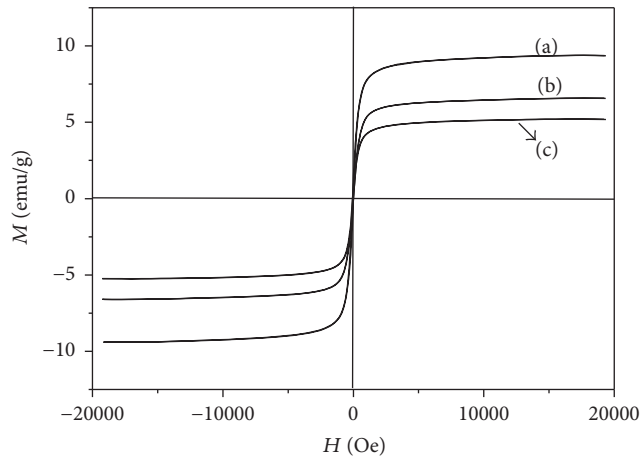

Figure 7: Magnetization curves of (a) Fe_3O_4/f-GO, (b) Fe_3O_4/GO, and (c) Fe_3O_4/RGO/PTX.

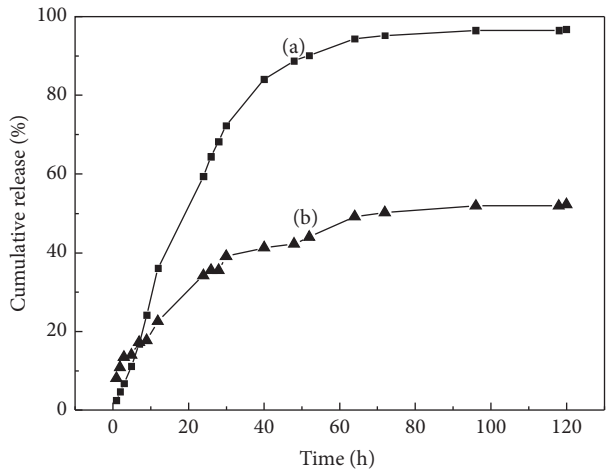

Figure 8: Release behavior of PTX from Fe_3O_4/RGO/PTX at (a) pH = 5.5 and (b) pH = 7.4.

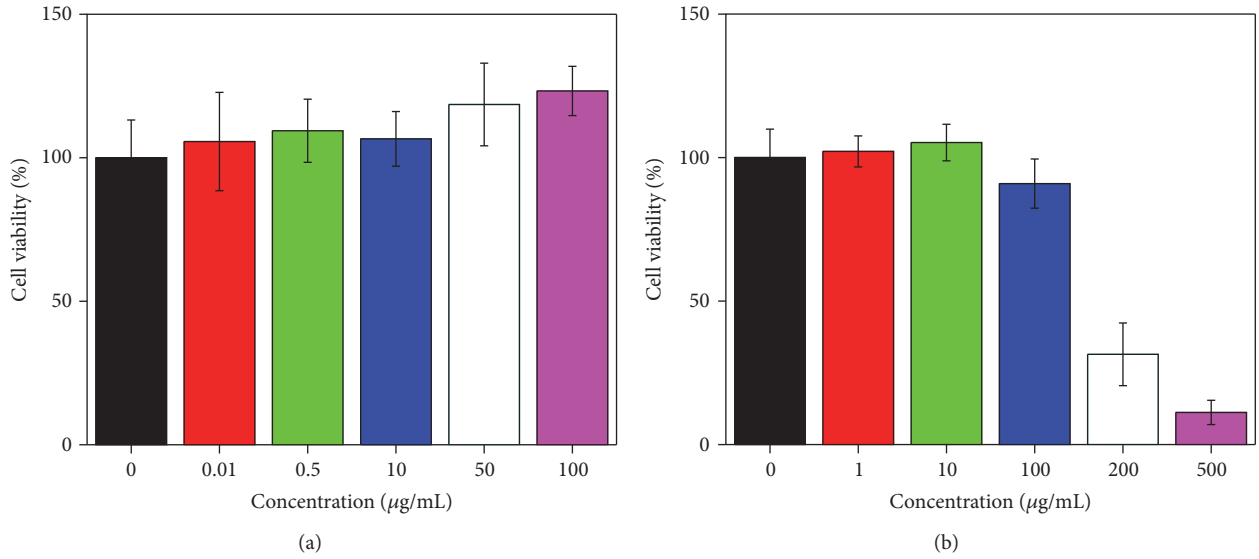

Figure 9: Histogram of cell viability is a function of (a) Fe_3O_4/RGO concentration and (b) Fe_3O_4/RGO/PTX concentration in culture media.

In Figure 8, a sustained PTX release at different pH values was observed from the Fe_3O_4/RGO/PTX. About 96.6% (Figure 8(a)) and 52.1% (Figure 8(b)) of PTX were released at pH = 5.5 and pH = 7.4 after 120 h. Moreover, the decreasing π-π stacking was the reason for rapid PTX release at pH = 5.5.

3.8. In Vitro Cytotoxicity Assay. In Figure 9(a), the free Fe_3O_4/RGO had no considerable cytotoxicity to MCF-7 cells. In Figure 9(b), with adding the Fe_3O_4/RGO/PTX, an obvious decrease in cell viability was observed. When the concentration of Fe_3O_4/RGO/PTX was 200 μg/mL, the cell viability was reduced to 31%. With adding the 500 μg/mL Fe_3O_4/RGO/PTX, the cell viability was rapidly reduced to 11%. It can be concluded that with increasing Fe_3O_4/RGO/PTX concentration the cell viability of MCF-7 decreased.

The cell viability results of products were also confirmed by fluorescence microscopy. The largest number of viable cells was exhibited in the control group (Figure 10(a)). With adding Fe_3O_4/RGO with different concentration (Figure 10(b), 1 μg/mL; Figure 10(c), 10 μg/mL; and Figure 10(d), 100 μg/mL), MCF-7 cells had no obvious morphological change.

The maximum viable cells were shown in the control group (Figure 11(a)). In Figure 11(b), with adding 100 μg/mL of Fe_3O_4/RGO/PTX, the number of viable MCF-7 cells reduced rapidly. When the concentration of PF127/Fe_3O_4/RGO/PTX increased to 200 and 500 μg/mL, few cells were observed (Figures 11(c) and 11(d)). It was confirmed that Fe_3O_4/RGO/PTX showed high antitumor activity for MCF-7 cells, which was ideal materials for tumor-targeted chemotherapy.

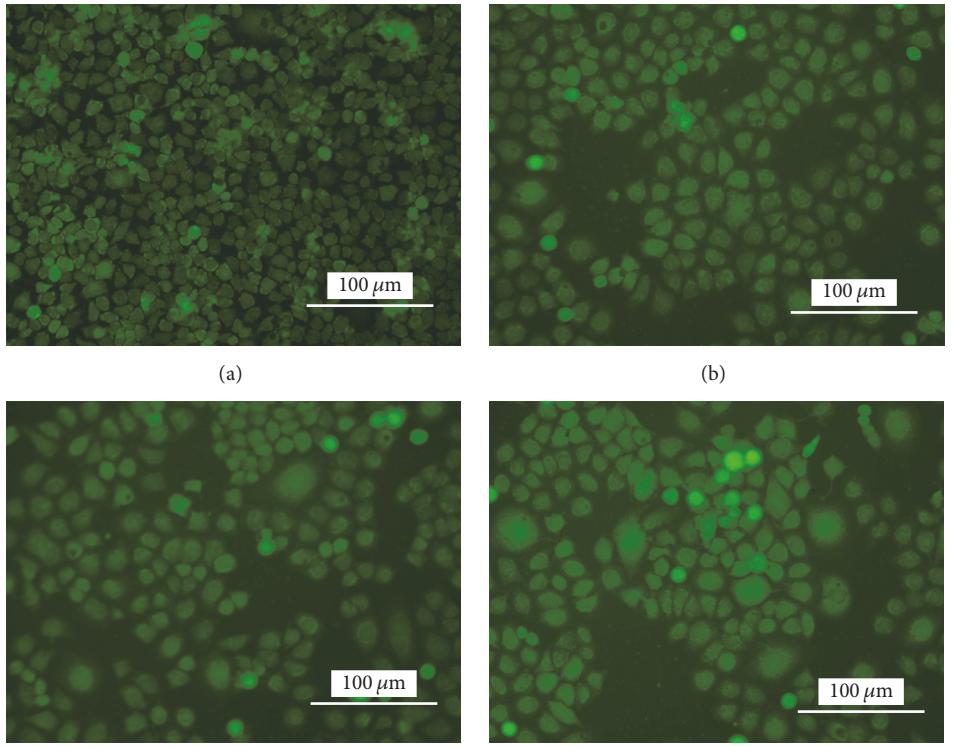

Figure 10: MCF-7 cells observed by fluorescence microscopy on (a) the control and (b–d) the Fe_3O_4/RGO of (b) 1 μg/mL, (c) 10 μg/mL, and (d) 100 μg/mL. Cell seeding density was 1×10^4 per well.

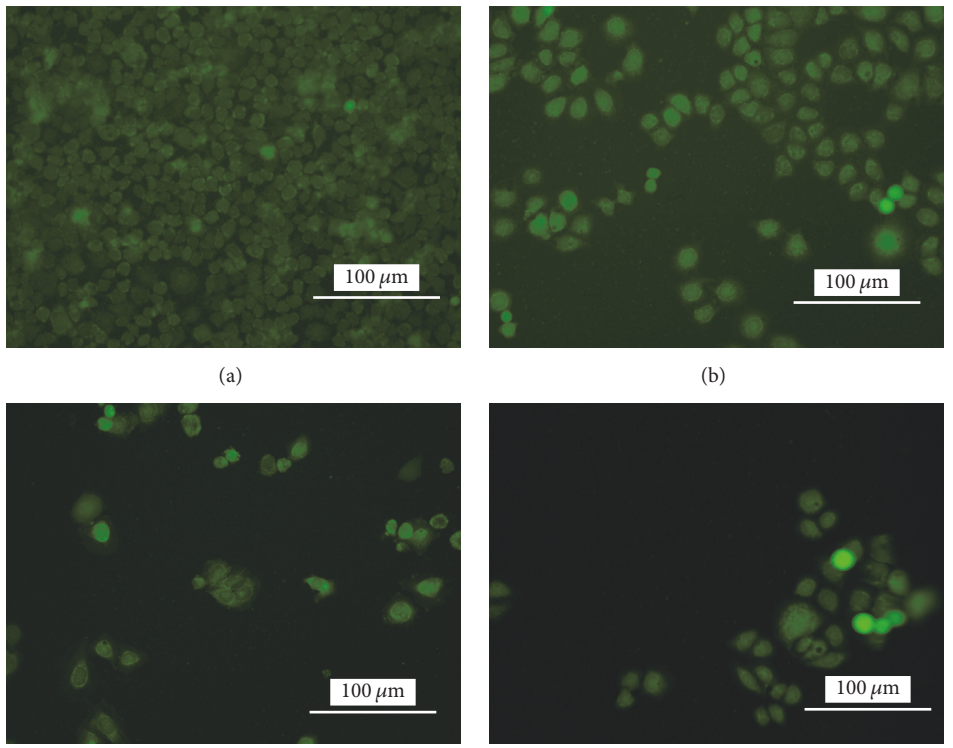

Figure 11: MCF-7 cells observed by fluorescence microscopy on (a) the control and (b–d) the Fe_3O_4/RGO/PTX of (b) 100 μg/mL, (c) 200 μg/mL, and (d) 500 μg/mL. Cell seeding density was 1×10^4 per well.

4. Conclusions

In conclusion, Fe_3O_4/RGO nanocomposites loading with PTX were successfully prepared. The method could be used for preparing other graphene-based nanocomposites. Moreover, the Fe_3O_4/RGO nanocomposites exhibited high drug loading efficiency and pH-dependent release, which was because of the π-π stacking and hydrophobic interactions between PTX and Fe_3O_4/RGO. With adding low concentration (200 μg/mL), the Fe_3O_4/RGO/PTX exhibited controlled release and inhibition of the growth of MCF-7 cells. Therefore, Fe_3O_4/RGO/PTX nanocomposites had potential application in tumor magnetically targeted therapy.

Conflicts of Interest

The authors declare that they have no conflicts of interest.

Acknowledgments

This work was supported by the sponsorship of Jiangsu Overseas Research & Training Program for University Prominent Young & Middle-Aged Teachers and Presidents and the research grants from the Natural Science Fund of Jiangsu Province (no. BK20130094).

References

[1] Y.-Z. Du, L. Wang, Y. Dong, H. Yuan, and F.-Q. Hu, "Characteristics of paclitaxel-loaded chitosan oligosaccharide nanoparticles and their preparation by interfacial polyaddition in O/W miniemulsion system," *Carbohydrate Polymers*, vol. 79, no. 4, pp. 1034–1039, 2010.

[2] J. H. Kim, J.-H. Lee, K.-S. Kim et al., "Intratumoral delivery of paclitaxel using a thermosensitive hydrogel in human tumor xenografts," *Archives of Pharmacal Research*, vol. 36, no. 1, pp. 94–101, 2013.

[3] C. Shu, E. M. B. Sabi-Mouka, W. Yang, Z. Li, and L. Ding, "Effects of paclitaxel (PTX) prodrug-based self-assembly peptide hydrogels combined with suberoylanilide hydroxamic acid (SAHA) for PTX-resistant cancer and synergistic antitumor therapy," *RSC Advances*, vol. 6, no. 103, pp. 100765–100771, 2016.

[4] W. J. Trickler, A. A. Nagvekar, and A. K. Dash, "A novel nanoparticle formulation for sustained paclitaxel delivery," *AAPS PharmSciTech*, vol. 9, no. 2, pp. 486–493, 2008.

[5] A. B. Dhanikula and R. Panchagnula, "Development and characterization of biodegradable chitosan films for local delivery of paclitaxel," *The AAPS Journal*, vol. 6, no. 3, pp. 88–99, 2004.

[6] Y. Wang, H. Xu, J. Wang, L. Ge, and J. Zhu, "Development of a thermally responsive nanogel based on chitosan-Poly(N- Isopropylacrylamide-co-Acrylamide) for paclitaxel delivery," *Journal of Pharmaceutical Sciences*, vol. 103, no. 7, pp. 2012–2021, 2014.

[7] X. Qian, W. Wang, W. Kong, and Y. Chen, "Organic-inorganic hybrid hollow mesoporous organosilica nanoparticles for efficient ultrasound-based imaging and controlled drug release," *Journal of Nanomaterials*, vol. 2014, Article ID 972475, 2014.

[8] Z. Zhao, Y. Li, and Y. Zhang, "Preparation and characterization of Paclitaxel loaded SF/PLLA-PEG-PLLA nanoparticles via solution-enhanced dispersion by supercritical CO2," *Journal of Nanomaterials*, vol. 2015, Article ID 913254, 2015.

[9] J. Emami, M. Rezazadeh, J. Varshosaz, M. Tabbakhian, and A. Aslani, "Formulation of LDL targeted nanostructured lipid carriers loaded with paclitaxel: a detailed study of preparation, freeze drying condition, and *in vitro* cytotoxicity," *Journal of Nanomaterials*, vol. 2012, Article ID 358782, 10 pages, 2012.

[10] A. Angelopoulou, E. Voulgari, E. K. Diamanti, D. Gournis, and K. Avgoustakis, "Graphene oxide stabilized by PLA-PEG copolymers for the controlled delivery of paclitaxel," *European Journal of Pharmaceutics and Biopharmaceutics*, vol. 93, Article ID 11879, pp. 18–26, 2015.

[11] C. Zhang, T. Lu, J. Tao, G. Wan, and H. Zhao, "Co-delivery of paclitaxel and indocyanine green by PEGylated graphene oxide: A potential integrated nanoplatform for tumor theranostics," *RSC Advances*, vol. 6, no. 19, pp. 15460–15468, 2016.

[12] S. Pattnaik, K. Swain, and Z. Lin, "Graphene and graphene-based nanocomposites: biomedical applications and biosafety," *Journal of Materials Chemistry B*, vol. 4, no. 48, pp. 7813–7831, 2016.

[13] S. Goenka, V. Sant, and S. Sant, "Graphene-based nanomaterials for drug delivery and tissue engineering," *Journal of Controlled Release*, vol. 173, no. 1, pp. 75–88, 2014.

[14] Y. Ye and X. Hu, "A pH-sensitive injectable nanoparticle composite hydrogel for anticancer drug delivery," *Journal of Nanomaterials*, vol. 2016, Article ID 9816461, 8 pages, 2016.

[15] W. Chen, P. Yi, Y. Zhang, L. Zhang, Z. Deng, and Z. Zhang, "Composites of aminodextran-coated Fe_3O_4 nanoparticles and graphene oxide for cellular magnetic resonance imaging," *ACS Applied Materials & Interfaces*, vol. 3, no. 10, pp. 4085–4091, 2011.

[16] L. Feng and Z. Liu, "Graphene in biomedicine: opportunities and challenges," *Nanomedicine*, vol. 6, no. 2, pp. 317–324, 2011.

[17] Y.-S. Huang, Y.-J. Lu, and J.-P. Chen, "Magnetic graphene oxide as a carrier for targeted delivery of chemotherapy drugs in cancer therapy," *Journal of Magnetism and Magnetic Materials*, vol. 427, pp. 34–40, 2017.

[18] H. Sereshti, S. Samadi, S. Asgari, and M. Karimi, "Preparation and application of magnetic graphene oxide coated with a modified chitosan pH-sensitive hydrogel: An efficient biocompatible adsorbent for catechin," *RSC Advances*, vol. 5, no. 13, pp. 9396–9404, 2015.

[19] J. Sun, Q. Liang, Q. Han, X. Zhang, and M. Ding, "One-step synthesis of magnetic graphene oxide nanocomposite and its application in magnetic solid phase extraction of heavy metal ions from biological samples," *Talanta*, vol. 132, pp. 557–563, 2015.

[20] E. Ma, J. Li, N. Zhao, E. Liu, C. He, and C. Shi, "Preparation of reduced graphene oxide/Fe_3O_4 nanocomposite and its microwave electromagnetic properties," *Materials Letters*, vol. 91, pp. 209–212, 2013.

[21] Ö. Metin, Ş. Aydoğan, and K. Meral, "A new route for the synthesis of graphene oxide-Fe_3O_4 (GO-Fe_3O_4) nanocomposites and their Schottky diode applications," *Journal of Alloys and Compounds*, vol. 585, pp. 681–688, 2014.

[22] G. Cheng, Y.-L. Liu, Z.-G. Wang, J.-L. Zhang, D.-H. Sun, and J.-Z. Ni, "The GO/rGO-Fe_3O_4 composites with good water-dispersibility and fast magnetic response for effective immobilization and enrichment of biomolecules," *Journal of Materials Chemistry*, vol. 22, no. 41, pp. 21998–22004, 2012.

[23] Z. Wang, C. Zhou, J. Xia et al., "Fabrication and characterization of a triple functionalization of graphene oxide with Fe_3O_4, folic acid and doxorubicin as dual-targeted drug nanocarrier," *Colloids and Surfaces B: Biointerfaces*, vol. 106, pp. 60–65, 2013.

[24] H. Hu, J. Yu, Y. Li, J. Zhao, and H. Dong, "Engineering of a novel pluronic F127/graphene nanohybrid for pH responsive drug delivery," *Journal of Biomedical Materials Research Part A*, vol. 100, no. 1, pp. 141–148, 2012.

[25] N. Mosallaei, M. R. Jaafari, M. Y. Hanafi-Bojd, S. Golmohammadzadeh, and B. Malaekeh-Nikouei, "Docetaxel-loaded solid lipid nanoparticles: preparation, characterization, *in vitro*, and *in vivo* evaluations," *Journal of Pharmaceutical Sciences*, vol. 102, no. 6, pp. 1994–2004, 2013.

[26] E. Omidinia, N. Shadjou, and M. Hasanzadeh, "(Fe_3O_4)-graphene oxide as a novel magnetic nanomaterial for non-enzymatic determination of phenylalanine," *Materials Science and Engineering C: Materials for Biological Applications*, vol. 33, no. 8, pp. 4624–4632, 2013.

[27] H. Jiang, L. Zhao, L. Gai, Y. Wang, Y. Hou, and H. Liu, "Conjugation of methotrexate onto dedoped Fe_3O_4/PPy nanospheres to produce magnetic targeting drug with controlled drug release and targeting specificity for HeLa cells," *Synthetic Metals*, vol. 207, Article ID 14989, pp. 18–25, 2015.

[28] L.-Z. Bai, D.-L. Zhao, Y. Xu et al., "Inductive heating property of graphene oxide-Fe_3O_4 nanoparticles hybrid in an AC magnetic field for localized hyperthermia," *Materials Letters*, vol. 68, pp. 399–401, 2012.

[29] X. Zhang, L. Hao, H. Sun et al., "Preparation of Epoxy-Functionalized Magnetic Polymer Nanospheres for Magnetically Targeted Radiotherapy," *Journal of Macromolecular Science, Part A Pure and Applied Chemistry*, vol. 52, no. 3, pp. 168–174, 2015.

[30] S. Alipour, H. Montaseri, and M. Tafaghodi, "Preparation and characterization of biodegradable paclitaxel loaded alginate microparticles for pulmonary delivery," *Colloids and Surfaces B: Biointerfaces*, vol. 81, no. 2, pp. 521–529, 2010.

[31] G. Wang, G. Chen, Z. Wei, X. Dong, and M. Qi, "Multifunctional Fe_3O_4/graphene oxide nanocomposites for magnetic resonance imaging and drug delivery," *Materials Chemistry and Physics*, vol. 141, no. 2-3, pp. 997–1004, 2013.